

Interferometric observations of η Carinae with VINCI/VLTI (Research Note)

P. Kervella

LESIA, UMR 8109, Observatoire de Paris-Meudon, 5, place Jules Janssen, F-92195 Meudon Cedex, France

Received ; Accepted

ABSTRACT

Context. The bright star η Carinae is the most massive and luminous star in our region of the Milky Way. Though it has been extensively studied using many different techniques, its physical nature and the mechanism that led to the creation of the Homunculus nebula are still debated.

Aims. We aimed at resolving the central engine of the η Carinae complex in the near-infrared on angular scales of a few milliarcseconds.

Methods. We used the VINCI instrument of the VLTI to recombine coherently the light from two telescopes in the K band.

Results. We report a total of 142 visibility measurements of η Car, part of which were analyzed by Van Boekel et al. (2003). These observations were carried out on projected baselines ranging from 8 to 112 meters in length, using either two 0.35 m siderostats or two 8-meter Unit Telescopes. These observations cover the November 2001 - January 2004 period.

Conclusions. The reported visibility data are in satisfactory agreement with the recent results obtained with AMBER/VLTI by Weigelt et al. (2006), assuming that the flux of η Car encircled within 70 mas reaches 56% of the total flux within 1400 mas, in the K band. We also confirm that the squared visibility curve of η Car as a function of spatial frequency follows closely an exponential model.

Key words. Stars: individual: η Car, Stars: circumstellar matter, Technique: interferometric

1. Introduction

η Carinae, the brightest example of the S Doradus class of stars, is the most massive, most luminous star in our region of the Milky Way. Over the last two hundred years η Car has shown many signs of violent activity, with in particular a spectacular eruption in the 1840s that created the Homunculus nebula. The study of η Car raises important questions about how the most massive stars may end their lives. The central object was studied by Weigelt & Ebersberger (1986) and Falcke et al. (1996) using speckle interferometry at an angular resolution of the order of 30 milliarcsecond (mas). This revealed a complex structure with several equatorial blobs at distances of 0.1 to 2 arcsec from the star, but the central engine remained unresolved. Long baseline interferometry, currently the only technique allowing the mas resolution necessary to resolve η Car, was recently applied to this star in the near- and mid-infrared domains by Van Boekel et al. (2003), Chesneau et al. (2005) and Weigelt et al. (2006). At the estimated distance of η Car of 2.3 kpc (Davidson & Humphreys 1997, Davidson et al. 2001, Smith 2006), one mas corresponds to 2.3 AU. We report in this Research Note the complete corpus of VINCI observations of η Car in the K band, including those discussed by Van Boekel et al. (2003).

2. Observations

The Very Large Telescope Interferometer (VLTI, Glindemann et al. 2003) has been operated by the European Southern Observatory on top of the Cerro Paranal, in Northern Chile since March 2001. For the present work, the light from η Car and its calibrators was collected either by two 0.35m VLTI Test Siderostats or two 8 m Unit Telescopes (UTs) without adaptive optics. It was subsequently recombined coherently in the VINCI instrument using a K band filter ($\lambda = 2.0 - 2.4 \mu\text{m}$).

We have observed η Car repeatedly over the period November 2001 to January 2004. This resulted in a total of 71 000 interferograms on this target, out of which 50% (35 639) were selected automatically by the pipeline. Approximately the same quantity of data were obtained on the calibrators. We used the standard VINCI data reduction pipeline (Kervella et al. 2004, version 3.1) to derive instrumental visibilities. The calibration of η Car's visibilities was done using well-known reference stars selected in the Bordé et al. (2002) and Cohen et al. (1999) catalogues, except β Car. The diameter of β Car was computed from an interferometric measurement obtained with the Intensity Interferometer (Hanbury Brown et al 1974). The original V band uniform disk (UD) angular diameter was converted into a K band uniform disk angular diameter ($\theta_{\text{UD}} = 1.54 \pm 0.10$ mas) using linear limb darkening coefficients from Claret et al. (2000). Thanks to the relatively low values of

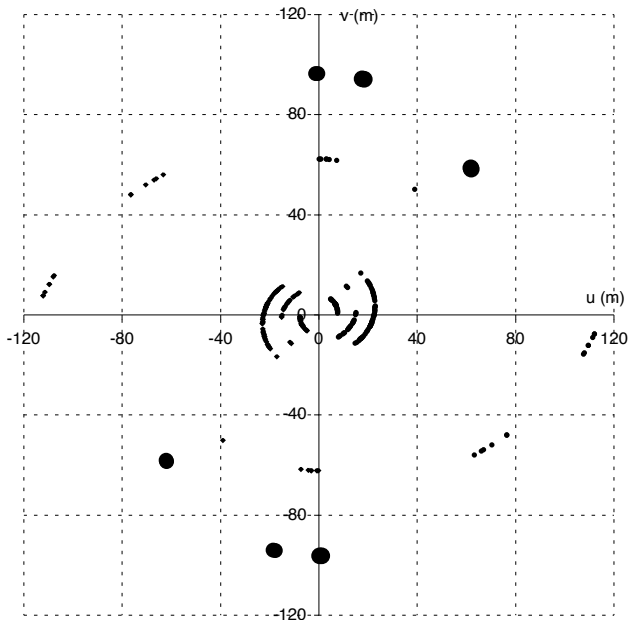


Fig. 1. (u, v) coverage of the η Car observations. Large spots represent the UT observations and small spots the siderostat observations (North is up and East is to the right).

η Car’s visibilities, the systematic uncertainty due to the calibrators is in general a small fraction of the total error bars.

The calibrated visibility values obtained on η Car are listed in Table 1. Thanks to the use of several different telescope configurations and to the supersynthesis effect, we were able to cover a broad range of baseline lengths and azimuth. The (u, v) coverage of our observations is presented in Figure 1.

3. Effective wavelength

The VINCI instrument has no spectral resolution and its band-pass corresponds to the K band filter (2.0-2.4 μm). It is thus important to compute the precise effective wavelength of the instrument in order to determine the spatial frequency of the observation. The true effective wavelength differs from the filter mean wavelength mainly because of the object spectrum shape, the detector quantum efficiency, and the fiber beam combiner transmission. To derive the effective wavelength of our observations, we computed a model taking into account η Car’s spectrum. The instrumental transmission of VINCI and the VLTI was measured on bright reference stars with the UTs (see Kervella et al. 2003 for details). Due to the extraordinarily dense, opaque stellar wind, the shape of the η Car spectrum in the infrared is different from the curve of a black body at the effective temperature of the central object. In particular, the flux is increasing by about 20% from 2.0 to 2.5 μm (Smith 2002). In our model, no spectral line either in emission or absorption has been taken into account, considering the relatively limited contribution of these spectral features to the total flux in the K band. Taking the average wavelength of this model spectrum gives an effective wavelength of $\lambda_{\text{eff}} = 2.196 \mu\text{m}$ for our η Car observations, slightly longer than the typical 2.179 μm value

for solar-type stars. We estimate the uncertainty on this effective wavelength to less than $\pm 0.5\%$, or $\pm 0.01 \mu\text{m}$.

4. Interferometric field of view

When injecting the light from an extended astronomical object into a single-mode fiber, the wavefront corrugation by the atmosphere (loss of coherence) is converted into photometric fluctuations. They are easily corrected during the data processing using the dedicated photometric channels of VINCI. Unfortunately, the restoration of coherence by spatial filtering comes at the expense of a very small field of view (FOV). It is well approximated by the diffraction pattern of a telescope whose size is the geometric mean of the apertures of the two telescopes. In the case of our homogeneous two-UT observations, the FOV is thus 70 mas in the K band. Considering the extension of the η Car complex, this limited FOV has an impact on the measured visibilities.

Guyon (2002) studied in detail this limitation for the interferometric observation of extended objects. One important conclusion is that the effective FOV depends on the seeing, and so does the visibility. This is particularly true when large telescopes are used without adaptive optics, as this was the case for our observations. While all the UTs are now equipped with MACAO adaptive optics systems (Arsenault et al. 2004), the early observations reported here were all obtained with atmosphere limited point spread functions. The atmospheric turbulence creates a large cloud of speckles on the fiber head, and incoherent light coming from separate parts of the object is coupled into the fiber, therefore reducing the contrast of the fringes. As a second order effect, different local seeing conditions for the two UTs could also slightly degrade the visibilities. In the case of small objects such as single stars, this effect is negligible, but η Car is surrounded by a large and bright envelope that is resolved by the UTs and contributes significantly to the light distribution within the FOV.

Practically, this means that the visibility measurements obtained with the UTs should be debiased from the seeing fluctuations. Unfortunately, this is not an easy task because the relationship between the speckle cloud size (defined by the seeing) and the flux coupled into the optical fiber is unknown. Tentatively, we mention as a first estimation of the UTs FOV the observatory seeing in the K band at the time of the observations. The seeing values from the Paranal DIMM, obtained at $\lambda = 0.5 \mu\text{m}$ have been converted to the K band assuming a classical $\lambda^{-6/5}$ dependance. Future comparisons of the visibility measurements reported in the present Note with results from other instruments should take into account their relative interferometric FOV.

On the other hand, the observations obtained with the 0.35m siderostats are in principle not affected by this bias because most of the η Car flux is coming from an area on the sky that is contained into the Airy pattern of these telescopes. Therefore, the obtained visibility is expected to be a faithful measurement of η Car’s intrinsic visibility in the 1.40 arcsec FOV of the siderostats. For the E0-G1 baseline, many visibility points have been obtained on different nights, with a broad range of seeing conditions. The fact that they give very consis-

tent visibility values is a confirmation that the FOV variation is negligible for the siderostats.

5. Discussion

Figure 2 shows a comparison of the VINCI squared visibilities with the AMBER model fitting result of Weigelt et al. (2006), represented as a thick curve. The VINCI squared visibilities show a strong decrease with increasing spatial frequencies, clearly indicating that the central source is resolved by the interferometer. The measurements obtained with the UTs, though in principle affected by an uncertainty due to the variation of the FOV with the seeing, are roughly consistent with the siderostat data obtained on comparable baselines. The simple model developed by Hillier et al. (2001, 2006), was adjusted by Weigelt et al. (2006) to the AMBER observations of η Car in the continuum at $\lambda = 2.174 \mu\text{m}$. This model is well reproduced by an exponential curve following the expression:

$$V^2 = 1.008 \exp(-0.016 s), \quad (1)$$

where $s = B/\lambda$ is the spatial frequency. Our wavelength reference is $\lambda = 2.196 \mu\text{m}$ (Sect. 3). On the same figure, the dashed curve is an exponential fit to the VINCI data:

$$V^2 = 0.322 \exp(-0.016 s). \quad (2)$$

The slopes (in logarithmic scale) of the VINCI data fit and the model representing the AMBER measurements are in excellent agreement. However, the ratio of the two (VINCI/AMBER) is $\rho^2 = 32\%$ in squared visibilities, translating into a factor $\rho = 56\%$ in visibilities. This ratio is constant with the spatial frequency, the signature of a fully resolved component.

To estimate the contribution of this extended component, we can consider the FOV of the two instruments. While the AMBER observations were obtained with the MACAO adaptive optics system in function (the FOV was thus ≈ 70 mas), the FOV of the VINCI siderostat observations was much larger, ≈ 1400 mas. From the observed ratio ρ between the visibilities measured by VINCI and AMBER, we can infer that 56% of the 1400 mas encircled K band flux of η Car comes from within the 70 mas point spread function of a single UT. This value is nicely consistent with the independent measurement by Van Boekel et al. (2003), based on adaptive optics observations with the NACO instrument, that gives an encircled energy of 57% within 70 mas. When corrected for the contribution of the extended emission, the visibilities measured by AMBER and VINCI are in excellent agreement.

A discussion of the shape of the dense stellar wind of η Car can be found in Smith et al. (2003) and Van Boekel et al. (2003). To improve the currently simplified spherical models, this observable appears highly desirable. The operating VLTI instruments are now routinely providing spectro-interferometric datasets on η Car (Weigelt et al. 2006; Chesneau et al. 2005), and the planned second generation will combine at least four telescopes, allowing to obtain rich data cubes at mas scales. This is an essential effort to follow the extremely fast evolution of η Car (Martin et al. 2006). In this context, the simple, two-telescopes, broadband VINCI data provide an interesting fiducial.

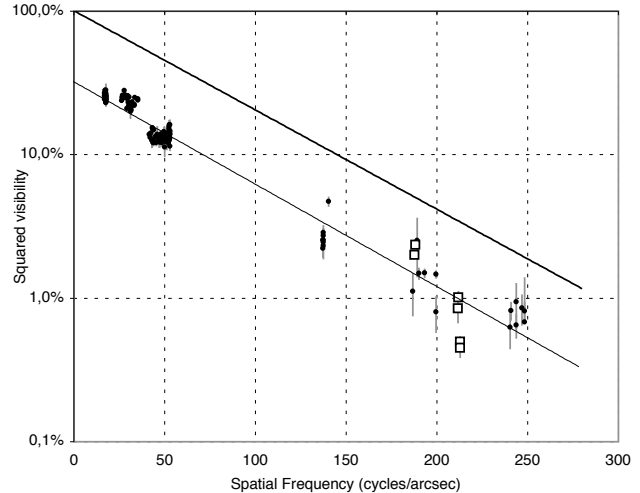


Fig. 2. Squared visibilities obtained on η Car with VINCI, compared to the model fitting result of Weigelt et al. (2006), represented as a solid curve. The UT data points are represented with open squares.

Acknowledgements. Based on observations made with ESO's VLT Interferometer at Cerro Paranal, Chile. The VINCI data were retrieved from the ESO/ST-ECF Archive. This research made use of the SIMBAD and VIZIER databases at the CDS, Strasbourg (France), and of NASA's Astrophysics Data System Bibliographic Services.

References

- Arsenault, R., Kervella, P., Donaldson, R., et al. 2004, *Proc SPIE*, 5490, 97
- Bordé, P., Coudé du Foresto, V., Chagnon, G., Perrin, G., 2002, *A&A*, 393, 183
- Chesneau, O., Min, M., Herbst, T., et al. 2005, *A&A*, 435, 1043
- Claret, A., 2000, *A&A* 363, 1081
- Cohen, M., Walker, R. G., Carter, B., et al. 1999, *AJ* 117, 1864
- Davidson, K., & Humphreys, R. M. 1997, *ARA&A*, 35, 1
- Davidson, K., Smith, N., Gull, T. R., Ishibashi, K., Hillier, D. J., 2001, *AJ*, 121, 1569
- Falcke, H., Davidson, K., Hofmann, K. H., Weigelt, G., 1996, *A&A*, 306, L17
- Glindemann, A., Argomedo, J., Amestica, R., et al. 2003, *ApSS*, 286, 1
- Guyon, O., 2002, *A&A*, 387, 366
- Hanbury Brown, R., Davis, J., Allen, L. R., 1974, *MNRAS*, 167, 121
- Hillier, D. J., Davidson, K., Ishibashi, K., & Gull, T. 2001, *ApJ*, 553, 837
- Hillier, D. J., Gull, T., Nielsen, K., et al. 2006, *ApJ*, 642, 1098
- Kervella, P., Thévenin, F., Ségransan, D., et al. 2003, *A&A*, 404, 1087
- Kervella, P., Ségransan, D. & Coudé du Foresto, V. 2004, *A&A*, 425, 1161
- Martin, J. C., Davidson, K., & Koppelman, M. D. 2006, *ApJ*, 132, 2717
- Smith, N., 2002, *MNRAS*, 336, 22
- Smith, N., Davidson, K., Gull, T. R., Hillier, J. 2003, *ApJ*, 586, 432
- Smith, N., 2006, *ApJ*, 644, 1151
- Van Boekel, R., Kervella, P., Schoeller, M., et al. 2003, *A&A*, 410, L37
- Weigelt, G. & Ebersberger, J., 1986, *A&A*, 163, L5

Weigelt, G., Kraus, S., Driebe, T., et al. 2006, A&A, in press,
astro-ph/0609715

Table 1. Squared visibilities measured with VINCI on η Car. The seeing in the *K* band at the time of the observation is given as the FOV with the UTs (see Section 4). *N* is the number of processed interferograms, *B* the baseline length, and Az. the azimuth angle of the projected baseline (North = 0°, East = 90°). The squared visibility values and error bars are expressed in percents. The statistical and systematic (from the calibrator star estimated angular size) error contributions are given separately.

JD -2.45 10 ⁶	Stations	FOV (")	<i>N</i>	<i>B</i> (m)	Az. (deg)	$V^2 \pm \text{stat.} \pm \text{syst.} (\%)$	Calibrators
2216.8643	UT1-UT3	0.15	35	96.350	179.21	0.50 ± 0.04 ± 0.01	γ^2 Vol
2216.8666	UT1-UT3	0.15	38	96.353	179.79	0.45 ± 0.07 ± 0.01	γ^2 Vol
2246.8287	UT1-UT3	0.37	108	95.906	10.59	1.01 ± 0.11 ± 0.03	γ^2 Vol. β Car
2246.8310	UT1-UT3	0.37	73	95.857	11.13	0.85 ± 0.18 ± 0.02	γ^2 Vol. β Car
2302.8796	E0-G0	1.40	183	14.264	102.33	21.19 ± 1.98 ± 0.05	HR 4630
2302.8851	E0-G0	1.40	147	14.139	104.15	19.96 ± 2.27 ± 0.05	HR 4630
2304.8225	UT1-UT3	0.12	55	85.216	46.55	2.36 ± 0.10 ± 0.05	HR 4546
2304.8239	UT1-UT3	0.12	203	85.033	46.87	2.00 ± 0.06 ± 0.04	HR 4546
2451.5692	E0-G1	1.40	83	62.115	6.82	2.22 ± 0.29 ± 0.07	θ Cen
2452.5393	E0-G1	1.40	29	62.229	0.10	2.73 ± 0.33 ± 0.07	HR 4050
2452.5426	E0-G1	1.40	142	62.227	0.90	2.87 ± 0.35 ± 0.08	HR 4050
2452.5504	E0-G1	1.40	253	62.209	2.84	2.32 ± 0.11 ± 0.06	HR 4050
2453.5382	E0-G1	1.40	30	62.228	0.49	2.45 ± 0.58 ± 0.07	HR 4050
2453.5480	E0-G1	1.40	224	62.207	2.93	2.54 ± 0.12 ± 0.08	HR 4050
2453.5521	E0-G1	1.40	113	62.190	3.93	2.54 ± 0.31 ± 0.08	HR 4050
2675.8452	B3-D1	1.40	139	21.815	97.97	12.89 ± 1.15 ± 0.04	HR 4050
2675.8537	B3-D1	1.40	221	21.540	100.74	13.11 ± 0.63 ± 0.04	HR 4050
2675.8599	B3-D1	1.40	111	21.331	102.80	12.36 ± 1.19 ± 0.04	HR 4050
2675.9027	B3-D1	1.40	237	19.763	117.77	12.09 ± 0.60 ± 0.03	HR 4050
2675.9095	B3-D1	1.40	108	19.501	120.31	12.67 ± 1.56 ± 0.03	HR 4050
2624.7905	B3-C3	1.40	466	7.932	37.64	26.38 ± 1.15 ± 0.01	HR 4050
2624.7948	B3-C3	1.40	373	7.940	39.05	24.84 ± 1.18 ± 0.01	HR 4050
2624.7988	B3-C3	1.40	390	7.947	40.37	24.35 ± 1.15 ± 0.01	HR 4050
2624.8400	B3-C3	1.40	144	7.986	53.48	25.79 ± 1.94 ± 0.01	HR 4050
2624.8581	B3-C3	1.40	356	7.978	59.09	25.61 ± 1.13 ± 0.01	HR 4050
2626.7952	B3-C3	1.40	333	7.950	40.99	22.91 ± 0.95 ± 0.01	HR 4050
2626.8014	B3-C3	1.40	337	7.959	42.97	23.34 ± 0.88 ± 0.01	HR 4050
2626.8141	B3-C3	1.40	349	7.974	47.06	23.31 ± 0.78 ± 0.01	HR 4050
2626.8453	B3-C3	1.40	468	7.983	56.82	25.40 ± 0.68 ± 0.01	HR 4050
2626.8496	B3-C3	1.40	421	7.981	58.15	26.07 ± 0.78 ± 0.01	HR 4050
2626.8539	B3-C3	1.40	381	7.977	59.49	25.79 ± 0.85 ± 0.01	HR 4050
2627.8450	B3-C3	1.40	235	7.982	57.58	24.50 ± 1.88 ± 0.01	HR 4050
2627.8496	B3-C3	1.40	283	7.978	58.99	25.06 ± 1.68 ± 0.01	HR 4050
2627.8539	B3-C3	1.40	313	7.974	60.32	25.28 ± 1.41 ± 0.01	HR 4050
2628.8599	B3-C3	1.40	277	7.960	62.97	24.13 ± 1.30 ± 0.01	HR 4050
2628.8650	B3-C3	1.40	147	7.950	64.53	26.82 ± 2.33 ± 0.01	HR 4050
2630.8258	B3-C3	1.40	139	7.986	54.17	24.57 ± 2.53 ± 0.01	HR 4050
2630.8601	B3-C3	1.40	372	7.949	64.71	23.47 ± 0.98 ± 0.01	HR 4050
2631.8387	B3-C3	1.40	205	7.978	59.00	24.13 ± 1.14 ± 0.01	HR 4050
2631.8428	B3-C3	1.40	90	7.974	60.25	24.40 ± 2.75 ± 0.01	HR 4050
2631.8780	B3-C3	1.40	151	7.888	70.97	24.46 ± 1.10 ± 0.01	HR 4050
2651.8286	B3-C3	1.40	435	7.867	72.53	27.06 ± 1.01 ± 0.01	HR 4050
2651.8534	B3-C3	1.40	195	7.740	80.02	25.86 ± 1.93 ± 0.01	HR 4050
2651.8619	B3-C3	1.40	421	7.684	82.62	25.79 ± 1.09 ± 0.01	HR 4050
2651.8702	B3-C3	1.40	332	7.625	85.15	24.29 ± 1.13 ± 0.01	HR 4050
2652.8461	B3-C3	1.40	185	7.767	78.64	28.03 ± 1.38 ± 0.01	HR 4050
2652.8640	B3-C3	1.40	142	7.650	84.11	26.78 ± 2.61 ± 0.01	HR 4050
2654.7670	B3-C3	1.40	88	7.984	56.25	24.93 ± 0.98 ± 0.01	HR 4050
2654.7718	B3-C3	1.40	272	7.982	57.73	23.59 ± 0.79 ± 0.01	HR 4050
2654.7769	B3-C3	1.40	120	7.977	59.31	28.27 ± 2.99 ± 0.01	HR 4050
2654.8272	B3-C3	1.40	71	7.837	74.59	26.90 ± 1.44 ± 0.01	HR 4050
2654.8311	B3-C3	1.40	335	7.818	75.77	24.46 ± 0.83 ± 0.01	HR 4050
2654.8483	B3-C3	1.40	435	7.720	80.99	26.62 ± 0.57 ± 0.01	HR 4050
2663.7817	B3-D1	1.40	212	23.795	68.34	15.19 ± 0.91 ± 0.05	HR 4050
2664.8213	B3-D1	1.40	66	23.197	81.14	12.54 ± 1.77 ± 0.04	HR 4050
2664.8519	B3-D1	1.40	187	22.493	90.57	14.36 ± 1.33 ± 0.05	HR 4050
2664.8561	B3-D1	1.40	187	22.379	91.88	14.41 ± 1.23 ± 0.05	HR 4050

Table 1. continued.

JD - 2.45 10 ⁶	Stations	FOV (")	<i>N</i>	<i>B</i> (m)	Az. (deg)	$V^2 \pm \text{stat.} \pm \text{syst.}$ (%)	Calibrators
2665.8654	B3-D1	1.40	227	22.032	95.70	12.34 ± 0.80 ± 0.04	HR 4050
2670.6898	B3-D1	1.40	320	23.946	45.81	13.89 ± 0.72 ± 0.05	HR 4050
2670.7270	B3-D1	1.40	263	23.985	57.49	16.20 ± 1.43 ± 0.06	HR 4050
2670.7312	B3-D1	1.40	287	23.976	58.77	14.12 ± 1.24 ± 0.05	HR 4050
2670.7567	B3-D1	1.40	217	23.845	66.57	16.16 ± 1.34 ± 0.06	HR 4050
2670.7661	B3-D1	1.40	177	23.762	69.40	15.69 ± 1.75 ± 0.05	HR 4050
2670.8071	B3-D1	1.40	172	23.154	81.81	13.67 ± 1.46 ± 0.04	HR 4050
2670.8121	B3-D1	1.40	158	23.051	83.35	14.16 ± 1.12 ± 0.05	HR 4050
2675.8452	B3-D1	1.40	139	21.815	97.97	12.89 ± 1.15 ± 0.04	HR 4050
2675.8537	B3-D1	1.40	221	21.540	100.74	13.11 ± 0.63 ± 0.04	HR 4050
2675.8599	B3-D1	1.40	111	21.331	102.80	12.36 ± 1.19 ± 0.04	HR 4050
2675.9027	B3-D1	1.40	237	19.763	117.77	12.09 ± 0.60 ± 0.03	HR 4050
2675.9095	B3-D1	1.40	108	19.501	120.31	12.67 ± 1.56 ± 0.03	HR 4050
2677.7022	B3-D1	1.40	458	23.993	55.70	14.67 ± 0.45 ± 0.05	HR 4050
2677.7094	B3-D1	1.40	466	23.982	57.94	14.56 ± 0.42 ± 0.05	HR 4050
2677.7168	B3-D1	1.40	463	23.961	60.21	13.88 ± 0.41 ± 0.05	HR 4050
2677.7542	B3-D1	1.40	389	23.684	71.59	12.47 ± 0.40 ± 0.04	HR 4050
2677.7617	B3-D1	1.40	357	23.590	73.85	12.07 ± 0.43 ± 0.04	HR 4050
2677.7698	B3-D1	1.40	377	23.473	76.31	12.32 ± 0.41 ± 0.04	HR 4050
2678.8376	B3-D1	1.40	485	21.795	98.17	13.91 ± 0.32 ± 0.04	HR 4050
2678.8447	B3-D1	1.40	450	21.565	100.49	13.19 ± 0.32 ± 0.04	HR 4050
2678.8519	B3-D1	1.40	386	21.326	102.85	12.32 ± 0.35 ± 0.04	HR 4050
2678.8914	B3-D1	1.40	389	19.881	116.62	14.84 ± 0.40 ± 0.04	HR 4050
2678.8979	B3-D1	1.40	208	19.634	119.02	15.38 ± 0.60 ± 0.04	HR 4050
2679.8071	B3-D1	1.40	387	22.594	89.36	13.53 ± 0.32 ± 0.04	HR 4050
2679.8149	B3-D1	1.40	256	22.386	91.81	12.34 ± 0.38 ± 0.04	HR 4050
2679.8216	B3-D1	1.40	285	22.197	93.92	12.87 ± 0.52 ± 0.04	HR 4050
2679.8580	B3-D1	1.40	355	21.018	105.82	13.10 ± 0.39 ± 0.04	HR 4050
2679.8644	B3-D1	1.40	113	20.789	108.00	13.88 ± 2.00 ± 0.04	HR 4050
2679.8941	B3-D1	1.40	193	19.674	118.63	15.15 ± 0.90 ± 0.04	HR 4050
2683.7023	B3-D1	1.40	206	23.954	60.78	11.48 ± 0.86 ± 0.03	HR 4050
2683.7105	B3-D1	1.40	128	23.916	63.31	13.09 ± 1.79 ± 0.03	HR 4050
2683.7171	B3-D1	1.40	169	23.875	65.31	12.65 ± 1.20 ± 0.03	HR 4050
2683.7274	B3-D1	1.40	430	23.792	68.45	12.83 ± 0.46 ± 0.03	HR 4050
2683.7347	B3-D1	1.40	408	23.719	70.63	12.55 ± 0.49 ± 0.03	HR 4050
2683.7421	B3-D1	1.40	437	23.631	72.89	13.48 ± 0.48 ± 0.03	HR 4050
2683.7746	B3-D1	1.40	431	23.094	82.72	12.31 ± 0.43 ± 0.03	HR 4050
2683.7819	B3-D1	1.40	467	22.936	84.96	13.01 ± 0.44 ± 0.03	HR 4050
2683.7888	B3-D1	1.40	444	22.775	87.10	12.72 ± 0.45 ± 0.03	HR 4050
2683.8185	B3-D1	1.40	243	21.963	96.43	12.14 ± 0.50 ± 0.03	HR 4050
2683.8254	B3-D1	1.40	105	21.749	98.64	13.00 ± 1.64 ± 0.03	HR 4050
2683.8581	B3-D1	1.40	192	20.621	109.59	12.09 ± 0.64 ± 0.03	HR 4050
2683.8658	B3-D1	1.40	449	20.334	112.31	13.39 ± 0.46 ± 0.03	HR 4050
2683.8736	B3-D1	1.40	256	20.040	115.10	12.48 ± 0.93 ± 0.03	HR 4050
2683.8928	B3-D1	1.40	172	19.306	122.25	14.13 ± 1.31 ± 0.04	HR 4050
2683.9008	B3-D1	1.40	272	18.998	125.39	13.21 ± 0.83 ± 0.03	HR 4050
2683.9065	B3-D1	1.40	275	18.784	127.63	13.83 ± 0.75 ± 0.04	HR 4050
2684.7819	B3-D1	1.40	211	22.874	85.81	13.05 ± 0.59 ± 0.01	HR 4050
2684.7929	B3-D1	1.40	80	22.607	89.21	11.33 ± 1.71 ± 0.01	HR 4050
2684.7992	B3-D1	1.40	118	22.442	91.16	12.58 ± 1.44 ± 0.01	HR 4050
2684.8310	B3-D1	1.40	198	21.476	101.38	12.17 ± 0.49 ± 0.01	HR 4050
2741.7918	B3-M0	1.40	55	84.580	131.47	1.12 ± 0.37 ± 0.04	HR 4526
2742.7684	B3-M0	1.40	70	90.319	122.20	0.80 ± 0.23 ± 0.03	HR 4526
2742.7849	B3-M0	1.40	52	85.714	129.50	2.52 ± 1.12 ± 0.09	HR 4526
2745.6829	B3-M0	1.40	36	112.435	93.90	0.68 ± 0.71 ± 0.01	HR 4831, HR 4546
2769.6173	B3-M0	1.40	104	112.447	93.89	0.81 ± 0.12 ± 0.01	HR 4831
2769.6249	B3-M0	1.40	94	110.408	96.36	0.65 ± 0.13 ± 0.01	HR 4831
2769.6299	B3-M0	1.40	111	109.049	98.01	0.82 ± 0.12 ± 0.01	HR 4831
2770.6169	B3-M0	1.40	82	111.816	94.66	0.85 ± 0.21 ± 0.01	HR 4831
2770.6224	B3-M0	1.40	64	110.358	96.42	0.94 ± 0.33 ± 0.01	HR 4831

Table 1. continued.

JD $-2.45 \cdot 10^6$	Stations	FOV (")	N	B (m)	Az. (deg)	$V^2 \pm \text{stat.} \pm \text{syst.}$ (%)	Calibrators
2770.6280	B3-M0	1.40	81	108.811	98.29	$0.63 \pm 0.19 \pm 0.01$	HR 4831
2786.6480	B3-M0	1.40	226	90.383	122.10	$1.47 \pm 0.08 \pm 0.05$	HR 4546
2786.6581	B3-M0	1.40	184	87.543	126.48	$1.50 \pm 0.10 \pm 0.05$	HR 4546
2786.6634	B3-M0	1.40	133	86.084	128.87	$1.49 \pm 0.13 \pm 0.05$	HR 4546
2790.5635	E0-G0	1.40	480	13.813	108.79	$25.20 \pm 0.39 \pm 0.01$	HR 4546
2790.5686	E0-G0	1.40	369	13.688	110.56	$21.89 \pm 0.40 \pm 0.01$	HR 4546
2790.5733	E0-G0	1.40	346	13.571	112.23	$23.13 \pm 0.47 \pm 0.01$	HR 4546
2790.6054	E0-G0	1.40	426	12.755	124.14	$26.06 \pm 0.59 \pm 0.01$	HR 4546
2790.6103	E0-G0	1.40	479	12.633	126.03	$28.03 \pm 0.58 \pm 0.01$	HR 4546
2790.6151	E0-G0	1.40	406	12.512	127.94	$24.87 \pm 0.56 \pm 0.01$	HR 4546
2791.4925	E0-G0	1.40	468	15.214	86.68	$25.02 \pm 0.30 \pm 0.01$	HR 4546
2791.4974	E0-G0	1.40	358	15.135	88.20	$22.31 \pm 0.36 \pm 0.01$	HR 4546
2791.5023	E0-G0	1.40	180	15.053	89.70	$22.05 \pm 0.85 \pm 0.01$	HR 4546
2791.5296	E0-G0	1.40	419	14.526	98.37	$23.30 \pm 0.35 \pm 0.01$	HR 4546
2791.5347	E0-G0	1.40	297	14.416	100.03	$21.75 \pm 0.45 \pm 0.01$	HR 4546
2791.5398	E0-G0	1.40	154	14.305	101.69	$20.42 \pm 0.96 \pm 0.01$	HR 4546
2791.5737	E0-G0	1.40	445	13.494	113.32	$25.73 \pm 0.59 \pm 0.01$	HR 4546
2791.5786	E0-G0	1.40	381	13.371	115.08	$24.49 \pm 0.59 \pm 0.01$	HR 4546
2791.5840	E0-G0	1.40	329	13.233	117.06	$20.99 \pm 0.58 \pm 0.01$	HR 4546
2791.6264	E0-G0	1.40	453	12.166	133.73	$25.88 \pm 0.58 \pm 0.01$	HR 4546
2791.6316	E0-G0	1.40	375	12.044	135.90	$25.05 \pm 0.61 \pm 0.01$	HR 4546
2791.6367	E0-G0	1.40	358	11.927	138.09	$23.81 \pm 0.58 \pm 0.01$	HR 4546
2977.8452	E0-G0	1.40	390	15.962	44.66	$24.45 \pm 0.41 \pm 0.01$	HR 4546
2977.8530	E0-G0	1.40	333	15.980	47.14	$24.03 \pm 0.41 \pm 0.01$	HR 4546
3011.7317	D0-H0	1.40	111	63.563	37.94	$4.72 \pm 0.37 \pm 0.07$	HR 4050